Title Page:

Enamel defects in the *Alpl*$^{-/-}$ murine model of infantile hypophosphatasia

Eri Yokoi [a*], Seiko Yamamoto-Nemoto [b]

[a] Department of Pediatric Dentistry, Nihon University Graduate School of Dentistry at Matsudo, Matsudo Chiba, Japan

[b] Department of Pediatric Dentistry, Nihon University School of Dentistry at Matsudo, Matsudo Chiba, Japan

*****Corresponding author. Department of Pediatric Dentistry, Nihon University Graduate School of Dentistry at Matsudo, 2-870-1 Sakaecho-Nishi, Matsudo, Chiba, 271-8587, Japan.

Tel: +81-47-360-9431

Fax: +81-47-360-9427

E-mail: maer13022@g.nihon-u.ac.jp (E. Yokoi).

Running title: EMPs expressions in hypophosphatasia mice

Abstract

Background/ purpose: Hypophosphatasia (HPP) is caused by mutations in the gene encoding tissue-nonspecific alkaline phosphatase (*ALPL*). HPP patients develop deficient calcification of bones and teeth including defects in cementum, dentin, and enamel and the characteristic premature loss of primary teeth. Here, we investigated the enamel defects of knockout ($Alpl^{-/-}$) mice compared with that of control wild type ($Alpl^{+/+}$) mice.

Methods/ results: No alkaline phosphatase (ALP) activity was detected by specific staining in the first molar germ of $Alpl^{-/-}$ mice on postnatal day 5. Hematoxylin and eosin staining revealed that the enamel layer in $Alpl^{-/-}$ mice was thin, undulated, and rugged. Furthermore, $Alpl^{-/-}$ mice had abnormal ameloblasts and the dentin-predentin layer blur and the abuttal not well defined. Some enamel defects matched non-homogeneous distribution of the enamel matrix proteins (EMPs); amelogenin (AMELX), ameloblastin (AMBN), and enamelin (ENAM), as shown by immunohistochemistry. Microarray analysis revealed that several expressions of genes related to enamel development were reduced in $Alpl^{-/-}$ mice. Furthermore, gene expressions of both *Ambn* and *Enam* were significantly lower in $Alpl^{-/-}$ mice than in $Alpl^{+/+}$ mice, as determined by quantitative real time PCR analysis. ($p < 0.05$).

Conclusion: Our study suggests that ALP may have involvement in EMPs and enamel defects in $Alpl^{-/-}$ mice is caused by ameloblasts disorder. Furthermore, our study advances elucidation of the mechanisms that underlie enamel development, and will support establish the causes of enamel defects of HPP patients.

Keywords: Hypophosphatasia; Alkaline phosphatase; Enamel defect; Enamel matrix protein; Tooth development

Introduction

Hypophosphatasia (HPP) is a hereditary skeletal disease caused by mutations of the gene encoding tissue-nonspecific alkaline phosphatase (*ALPL*) [1]. Four types of human alkaline phosphatase (ALP) are distinguished: tissue-nonspecific, intestinal, placental, and germ cell type. Alkaline phosphatase, tissue-nonspecific isozyme (TNSALP) is involved in bone formation during the development and mineralization of the human skeleton. TNSALP is an ectoenzyme attached to the cell membrane by a glycosylphosphatidylinositol anchor. In the extracellular matrix, TNSALP hydrolyzes physiological substrates such as inorganic pyrophosphate (PP_i), pyridoxal-5′-phosphate, and phosphoethanolamine. PP_i inhibits mineralization and accumulates, in the absence of TNSALP. This results in incomplete mineralization of hard tissues. Thus, TNSALP is considered to be involved in the strict regulation of mineralization.

HPP is classified into six characteristic forms: perinatal, perinatal benign, infantile, childhood, adult, and odonto-HPP [2]. The clinical severity of HPP spans a wide range of symptoms and varies from lethal perinatal to mild odonto-HPP confined to tooth abnormalities. *ALPL* gene mutations result in insufficient TNSALP activity, leading to hypomineralization, osteomalacia, or rickets, often causing death early in life. Although TNSALP is expressed in various tissues, HPP symptoms are observed primarily in the bones and teeth. However, the biological and pathological mechanisms underlying calcification in HPP have not been determined.

Oral manifestations of HPP include a characteristic premature loss of primary teeth; dysplasia or aplasia of the cementum have also been reported. Deficient attachment of the tooth root to the surrounding dentoalveolar tissues is frequently cited as an explanation for these abnormalities. Dentin defects are not consistently noted in human case reports. Pulp chamber expansion and thin dentin have been reported in some studies, while others declared no HPP effect on dentin formation. Enamel hypoplasia and severe tooth caries have also been reported in HPP patients [3, 4]. These oral symptoms are common in all forms of HPP [5].

Recently, many studies have been conducted using the HPP mouse model ($Alpl^{-/-}$) to

clarify the mechanisms underlying the abnormal calcification in hard tissue accompanying *Alpl* gene mutations [6,7]. Several reports contained histological examination of the dentin and cementum defects in $Alpl^{-/-}$ mice [8-10]. However, only a few reports concern enamel defects in this model [11] and enamel defects during HPP are as yet uncharacterized. Therefore, in this study, we examined enamel development in the $Alpl^{-/-}$ mice to gain further insight into this potentially deleterious disease.

Materials and methods

Animals

All animal experiments were reviewed and approved by the Nihon University Intramural Animal Experiment Committee (No. AP12MD005). Heterozygous ($Alpl^{+/-}$) mice were obtained from the Nippon Medical School (Tokyo, Japan). Wild type ($Alpl^{+/+}$), $Alpl^{+/-}$, and knockout ($Alpl^{-/-}$) mice were obtained by breeding $Alpl^{+/-}$ mice [7], according to the Guidelines of the Nihon University Intramural Animal Use. $Alpl^{-/-}$ mice display a severe growth defect and experience repeated convulsions caused by metabolic disorder of pyridoxal phosphate, a TNASLP substrate, and die at ~2-weeks old. Because of these characteristics, these mice are regarded as a model of severe infantile form of HPP as described [12]. Mice were classified by genotyping. PCR was performed using *Alpl* primers (forward primer: 5′-AGTCCGTGGGCATTGTGACTA-3′; reverse primer: 5′-TGCTGCTCCACTCACGTCGAT-3′) [13] with LA Taq® (Takara, Tokyo, Japan). In our study, mice were euthanized left on the ice and collected samples for each experiments.

Cell culture and RNA preparation for microarray analysis

$Alpl^{+/+}$ (n=1) and $Alpl^{-/-}$ (n=1) mice were used on postnatal day 8. The heads were immediately dissected under a dissection microscope. First molars (M1s), second molars

(M2s), and incisors were pulled out from the maxillary and mandibular bone, and their dental pulp dissected. Each isolated dental pulp sample was chopped into about 1 mm^3 squares by scissors, placed into 6-well cell culture dishes, and incubated at 37 °C in 5% CO_2 in dulbecco's Modified Eagle Medium (DMEM; Wako, Osaka, Japan) supplemented with 20% fetal bovine serum (FBS), 1% penicillin/streptomycin/amphotericin B suspension (Wako), and 1% GlutaMAX™-1 (Gibco® by Thermo Fisher Scientific, Kanagawa, Japan). The primary culture was maintained for 14 days. The outgrowth of an adherent cell population was harvested and sub-cultured as passage 2. Cell morphology was observed under a light microscope. When the cells had reached 80% confluence, total RNA was extracted using miRNeasy® Mini Kit (Qiagen, Tokyo, Japan). RNA quality was verified with Agilent 2100 Bioanalyzer (Agilent Technologies, Foster City, CA, USA).

Microarray analysis

We carried out exhaustive microarray gene analysis of cultured cells of dental pulp from postnatal day 8 *Alpl*$^{+/+}$ and *Alpl*$^{-/-}$ mice with SurePrint G3 Mouse Gene Expression Microarray 8 × 60 K (Entrez Gene; 39,430; Agilent Technologies). Microarray hybridization was carried out with total RNA (50 ng) according to the Agilent Expression Array protocols. Cy3 labeled cRNA synthesis was performed by Low Input Quick Amp Labeling Kit, one-color (Agilent Technologies). Hybridization was worked with 0.6 μg Cy3 labeled cRNA as described [14]. The standardization between arrays was performed by global normalization (mean value) excluding higher 2 % and lower 2 % of their signal intensities.

Histological analysis

Alpl$^{+/+}$ (n=5) and *Alpl*$^{-/-}$ (n=5) mice were used the mandibular right first molar (M1) germs of postnatal day 5. The heads were fixed in 4% paraformaldehyde phosphate buffer solution (PFA; Wako) and embedded in paraffin. Sagittal sections (5 μm thick) were cut, and stained with hematoxylin and eosin (H&E) according to conventional techniques.

ALP activity staining

ALP activity was performed on histological sections of the craniofacial regions of postnatal day 5 *Alpl*$^{+/+}$ (n=5) and *Alpl*$^{-/-}$ (n=5) mice. Heads were fixed in 4% PFA (Wako) for 24 h at 4 °C. Tissues were washed with phosphate buffered saline (PBS; Wako) and then embedded in optimal cutting temperature (OCT) compound (Tissue-Tek, Sakura Finetechnical Co., Ltd., Tokyo, Japan). Samples were stored at –80 °C. The thin coronal sections (5 μm thick) were prepared using Leica CM1520 cryostat (Leica Microsystems, Wetzlar, Germany) and mounted on glass slides. The sections were washed in PBS and rinsed with 0.2 M Tris-HCl (pH 8.9). The sections were placed in a solution containing dissolved in 25ml distilled water (DW) with 5mg naphthol AS-MX phosphoric acid disodium salt (N-5000; Sigma, Tokyo, Japan) , and dissolved in 25ml 0.2 M Tris-HCl (pH 8.9), 1 mM MgCl2 (Wako), and 20 μM ZnCl2 (Wako) with 30mg Fast Violet B salt (F-1631; grade IV, 98%, Sigma), these were incubated at 37 °C for 30–60 min [6]. Methyl green stain solution (1%; pH 4.0) (MUTO, Tokyo, Japan) was used for counterstaining.

Immunohistochemistry

We next used immunohistochemistry (IHC) to assess the distribution and prevalence of EMPs in M1 germs of postnatal day 5 *Alpl*$^{+/+}$ and *Alpl*$^{-/-}$ mice. IHC was performed according to a Genostaff protocol (Tokyo, Japan). Heads of postnatal day 5 mice (n=1 for each group) were dissected and fixed in 4% PFA (Wako) for 16 h at 4 °C. For IHC, the following primary rabbit antibodies were used: amelogenin (AMELX) (LS-C156308; 0.4 μg/mL; polyclonal; LifeSpan BioSciences, Seattle, WA, USA); ameloblastin (AMBN) (bs-12467R; 2.0 μg/mL; polyclonal; Bioss Inc., Woburn, MA, USA); enamelin (ENAM) (serum dilution 1:5,000; a gift from Dr. T. Uchida, Hiroshima University, Japan) [15], negative control (NC) for AMELX and AMBN (X0936; each 0.4 μg/mL and 2.0 μg/mL

rabbit Ig; Dako A/S, Glostrup, Denmark), and for ENAM (R9133; normal rabbit serum, Sigma, Tokyo, Japan). Tissue sagittal sections (5 μm) were deparaffinized in xylene, and rehydrated through ethanol series and PBS. Antigen retrieval was performed by enzyme treatment with 10 μg/mL Proteinase K at 37 °C for 10 min (AMELX), heat treatment at 80 °C (AMBN) or at 90 °C (ENAM) for 40 min with citrate buffer, pH 6.0. Endogenous peroxidase activity was blocked with 0.3 % H_2O_2 in methanol at room temperature for 30 min, followed by incubation with G-Block (GB-01; Genostaff) at room temperature for 10 min and avidin/biotin blocking kit (SP-2001; Vector Labs, California, USA). The sections were incubated with primary antibody solutions at 4 °C overnight. They were washed twice with Tween-Tris-buffered saline, then with Tris-buffered saline, 5 min at room temperature each, and incubated with biotin-conjugated goat anti-rabbit IgG (E0432; dilution 1:600; polyclonal; Dako) for 30 min at room temperature. This was followed by the addition of peroxidase-conjugated streptavidin (426062; Nichirei, Tokyo, Japan) for 5 min. Peroxidase activity was visualized with diaminobenzidine substrate. The sections were mounted with Malinol (MUTO).

Quantitative real time PCR

Alpl$^{+/+}$ (n=5) and *Alpl*$^{-/-}$ (n=5) mice were used on postnatal day 5. Total RNA was extracted from M1 germs using miRNeasy Micro Kit (Qiagen). Total RNA (50 ng) were converted into cDNA with PrimeScript™ High Fidelity RT-PCR Kit (Takara). Quantitative real time PCR (qPCR) reactions were performed with TaqMan® Universal Master Mix II (Thermo Fisher Scientific) using QuantStudio™ 6 Flex Real-Time PCR System (Thermo Fisher Scientific), according to manufacturer's recommendations. The following primer and Taqman probe combinations (Thermo Fisher Scientific) were used: amelogenin (*Amelx*), Mm00711642_m1; ameloblastin (*Ambn*), Mm00477486_m1); enamelin (*Enam*), Mm00516922_m1; glyceraldehyde-3-phosphate dehydrogenase (*Gapdh*), Mm99999915_g1. qPCR gene expression data were calculated by the $2^{-\Delta\Delta Ct}$ method with *Gapdh* as the internal control, as follows: $\Delta\Delta Ct = (Ct_{target} - Ct_{Gapdh})_{Alpl-/-} - (Ct_{target} - Ct_{Gapdh})_{Alpl+/+}$ [16, 17], with *C*t

as the appropriate cycle threshold.

Statistical analysis

Statistical differences between gene expression in *Alpl*$^{+/+}$ and *Alpl*$^{-/-}$ mice were analyzed by Mann-Whitney U test using IBM SPSS Statistics software (version 19.0, Armonk, NY, USA). The data are presented as mean ± SD. A value of $p < 0.05$ was considered statistically significant. To ensure reproducibility, experiments were repeated at least three times.

Results

Microarray analysis of gene expression in dental pulp of Alpl$^{+/+}$ *and Alpl*$^{-/-}$ *mice*

After data mining, 3,559 genes had greater than two-fold in their expression changes, by statistical group comparison between *Alpl*$^{+/+}$ and *Alpl*$^{-/-}$ mice. Among them, an *Alpl* displayed the most decreased expression (log2 ratio; -7.32) in *Alpl*$^{-/-}$ mice in compared with *Alpl*$^{+/+}$ mice. Otherwise, genes associated with tooth development were selected (Table 1) [18-20]. Among the enamel matrix proteins (EMPs)-encoding genes; *Amelx*, *Ambn*, and *Enam* [21], the expression of *Amelx* was most reduced ($\log_2$ ratio = -6.21) in *Alpl*$^{-/-}$ mice compared with controls, followed by *Enam* ($\log_2$ ratio = -2.72), and *Ambn* ($\log_2$ ratio = -1.34). Expression of amelotin (*Amtn*) and odontogenic ameloblast-associated (*Odam*) genes [22-24] was reduced in *Alpl*$^{-/-}$ mice. Similarly, kallikrein-related peptidase 4 (*Klk4*) [25], dentin sialophosphoprotein (*Dspp*) [26], integrin binding sialoprotein (*Ibsp*) [27], and sonic hedgehog (*Shh*) [28] were also reduced in the *Alpl*$^{-/-}$ mice, at least two-fold. No significant difference in expression, less than two-fold, was observed for other well-known genes of tooth development; dentin matrix protein 1 (*Dmp1*) [29], matrix metallopeptidase 20 (*Mmp20*) [25] and collagen type I (*Col1*) [30].

Histological analysis of M1 tooth germs of Alpl$^{+/+}$ and Alpl$^{-/-}$ mice

H&E staining revealed an apparently similar tooth germ development in *Alpl*$^{-/-}$ and *Alpl*$^{+/+}$ mice (Fig. 1). On postnatal day 5, M1 tooth germs in each group were at the late bell stage, with enamel organ covering the dental papilla. The enamel and dentin were layered on the crown but not at the root. The exterior form of M1s at late bell stage was almost the same in *Alpl*$^{+/+}$ and *Alpl*$^{-/-}$ mice (overview: Fig. 1A, D; details: remaining panels). Enamel was surrounded by ameloblasts, stratum intermedium, and stellate reticulum that comprise the enamel organ. Ameloblasts were at a secretory stage, with elongated and tall cell bodies, and the nucleus located in the distal cell body. Further, ameloblasts were covered with flat stratum intermedium around which stellate reticulum had spread. Subjacent to the enamel organ, dental papilla consisted of dentin, predentin, and odontoblasts. Dental pulp spread below the odontoblasts. Compared with *Alpl*$^{+/+}$ mice, the enamel of *Alpl*$^{-/-}$ mice was thinner (Fig. 1A, D). Whereas ameloblasts of *Alpl*$^{+/+}$ mice uniformly covered the enamel, some ameloblasts in *Alpl*$^{-/-}$ mice had irregular shape, with disturbed nuclear polarity (Fig. 1B, C, E). Interestingly, while the enamel layer of *Alpl*$^{+/+}$ mice was uniform, that of *Alpl*$^{-/-}$ mice was rippling or uneven (Fig. 1B, C, F). Dentin and predentin layers of *Alpl*$^{-/-}$ mice tended to be non-uniform and not well defined compared with those of *Alpl*$^{+/+}$ mice (Fig. 1B, C, E, F).

ALP activity in craniofacial regions of Alpl$^{+/+}$ and Alpl$^{-/-}$ mice

Craniofacial regions of postnatal day 5 mice were analyzed histochemically for ALP activity (Fig. 2). In *Alpl*$^{+/+}$ animals, ALP was not detected in the soft tissues, such as the tongue and cheek muscles, but its activity was high in the hard tissues, such as the alveolar bone, trabecular bone, cortical plate and developing tooth germs (Fig. 2A). On closer inspection, ALP activity was observed in the cells of stratum intermedium, stellate reticulum, odontoblasts, and dental pulp, but not in ameloblasts, enamel, and dentin (Fig. 2B). In contrast, no ALP signal was detected in *Alpl*$^{-/-}$ mice (Fig. 2D, C).

IHC detection of AMELX, AMBN, and ENAM in $Alpl^{+/+}$ and $Alpl^{-/-}$ mice

AMELX, AMBN and ENAM antibody detected specific signals in roughly corresponding tissue areas in $Alpl^{+/+}$ and $Alpl^{-/-}$ mice (Fig. 3–5).

The AMELX signal was pronounced in the enamel (Fig. 3). The signal was much weaker than enamel compared with the secretory ameloblast cell bodies, and was absent in the dental papilla (Fig. 3A–C, G–I). AMELX IHC staining revealed that enamel layer in $Alpl^{-/-}$ mice was disturbed and unevenly localized, with no staining in the enamel-lacking region (Fig. 3G–I). These areas of aberrant staining partly overlapped with the enamel defects seen in H&E staining (Fig. 2).

AMBN IHC staining was slightly weaker and irregular in $Alpl^{-/-}$ mice compared with $Alpl^{+/+}$ mice (Fig. 4). The AMBN antibodies reacted with the enamel and secretory ameloblast cell bodies to the same extent in $Alpl^{+/+}$ and $Alpl^{-/-}$ mice. In contrast, AMBN signal was not apparent in the dentin, predentin, odontoblasts, and pulp (Fig. 4A–C, G–I). Strong staining at the basal side of ameloblast cell bodies was observed, but not in the abnormal ameloblasts in $Alpl^{-/-}$ mice (Fig. 4H).

ENAM signal was pronounced in the enamel and weaker in the ameloblast cell bodies (Fig. 5). In particular, the IHC staining of enamel layer was more pronounced on the ameloblast side and accumulated on the dentin side (Fig. 5A–C, G–I). The section lacking enamel layer in $Alpl^{-/-}$ mice did not react with anti-ENAM antibodies (Fig. 5H). Furthermore, ENAM signal in the enamel in $Alpl^{-/-}$ mice was observed along the wavy/bumpy portion detected in H&E staining (Fig. 5I).

qPCR analysis of amelogenesis-associated genes in $Alpl^{+/+}$ and $Alpl^{-/-}$ mice

We then examined the expression of amelogenesis-related genes, *Amelx*, *Ambn*, and *Enam*, in $Alpl^{+/+}$ and $Alpl^{-/-}$ mice in greater detail. We used qPCR to quantify mRNA levels of these genes (Fig. 6). After normalization with Gapdh, their values of *Amelx*, *Ambn*, *Enam*

were 0.92 ± 0.22, 0.77 ± 0.17, and 0.88 ± 0.17 respectively in *Alpl*$^{+/+}$ mice, 0.87 ± 0.22, 0.39 ± 0.12, and 0.50 ± 0.14 respectively in *Alpl*$^{-/-}$ mice. The expression of *Ambn* and *Enam* was significantly lower in *Alpl*$^{-/-}$ mice than in *Alpl*$^{+/+}$, however there was no significant difference in expression of *Amelx* between *Alpl*$^{+/+}$ and *Alpl*$^{-/-}$ mice (*Ambn*, $p < 0.05$ and *Enam*, $p < 0.01$).

Discussion

In this study, we focused on the enamel defects in *Alpl*$^{-/-}$ mice. Following an extensive microarray analysis, we conducted biochemical and histological examination of mutant and control mouse M1s on postnatal day 5 to assess ALP activity and the distribution of AMELX, AMBN, and ENAM proteins to clarify their role in early stages of enamel mineralization [31]. H&E staining revealed that the enamel of *Alpl*$^{-/-}$ mice had an undulating shape, was thinner and non-uniform than in control mice (Fig. 1). Some *Alpl*$^{-/-}$ M1 regions showed irregularity in ameloblast alignment and lacked enamel layers. Moreover, IHC staining for AMELX, ENAM, and AMBN revealed similar distribution of these proteins in *Alpl*$^{-/-}$ and *Alpl*$^{+/+}$ mice (Figs. 3–5). The expression of *Ambn* and *Enam* was significantly lower in *Alpl*$^{-/-}$ mice than in *Alpl*$^{+/+}$, as assessed by qPCR (Fig. 6). These results revealed that ameloblasts in *Alpl*$^{-/-}$ animals are non-uniform, with EMPs characterized by distributional and quantitative abnormalities.

TNSALP has been the subject of research for many years. Even though it has been established that TNSALP is crucially involved in the process of bone and tooth mineralization, many issues remain unresolved. HPP is caused by functional defects in TNSALP associated with mutations in the *ALPL* gene, with unmetabolized PP_i (one of the substrates of TNSALP) inhibiting crystalline formation of hydroxyapatite [1, 2]. Absence of enamel formation has been reported in a previous study of *Alpl*$^{-/-}$ mice, specifically, defects of enamel rods and inter-rods structures [11]. In addition, alveolar bone mineralization defects, complete lack of dentin mineralization, enlarged pulp chambers, noticeably short root lengths, and cementum defects were reported [10]. Thus, TNSALP is involved in craniofacial skeletal development

and its absence results in enamel, dentin, and cementum defects in murine HPP [32]. In this study, we analyzed ALP activity in *Alpl*$^{-/-}$ mice on postnatal day 5. No activity was detected in the alveolar bone and dental buds at bell stage in contrast with *Alpl*$^{+/+}$ mice (Fig. 2A, C). This supports the notion that the lack of TNSALP affects the developmental of dental buds.

ALP activity was detected in stellate reticulum, stratum intermedium, odontoblasts, and dental pulp but not in ameloblasts in postnatal day 5 *Alpl*$^{+/+}$ mice (Fig. 2B), in contrast with *Alpl*$^{-/-}$ mice where ALP activity was not observed at all (Fig. 2D). H&E staining revealed abnormal ameloblasts in *Alpl*$^{-/-}$ mice, in agreement with what has been described before. Yadav *et al.* reported that TNSALP was expressed in the stratum intermedium and odontoblasts, but not in ameloblasts, on post-coital day 15 and postnatal day 4 in *Alpl*$^{+/+}$ [11]. Similarly, Wise and Fan evidenced that ALP activity transitioned from stellate reticulum to stratum intermedium, to the ameloblast, and finally the enamel, in M2 of 3-16 days old rat [33]. These authors also showed a migratory pattern of ALP, and they said that the instance may lead to the ALP function on enamel organ. Furthermore, Yadav *et al.* reported that a recombinant TNSALP enzyme replacement therapy prevented the enamel defect of *Alpl*$^{-/-}$ mice [11]. Additionally recent study recovered that stratum intermedium highly associated with cell differentiation processes of ameloblasts in inner dental epithelium [34-36]. Thus, we conclude that TNSALP strongly correlates with the development of dental organ, such as stratum intermedium, odontoblasts, and ameloblasts, and EMPs secreted by the ameloblasts. Further, the lack of TNSALP triggers the enamel defect in *Alpl*$^{-/-}$ mice.

Mineralization of enamel and dentin involves an interplay of various proteins. AMELX is an important factor influencing the thickness of enamel layer during enamel formation. AMBN and ENAM play roles in the differentiation to ameloblasts, and amelotin (AMTN) is involved in the post-secretory or maturation stage of ameloblasts. AMTN and odontogenic ameloblast-associated (ODAM) have been suggested to be associated with enamel development [22-24]. Kallikrein-related peptidase 4 (KLK4) and matrix metallopeptidase 20 (MMP20) degrade the enamel protein and are thought to play a role in tooth enamel formation. Furthermore, KLK4 affects the post-secretory or maturation stage of ameloblasts, while MMP20 is associated with the secretory stage of ameloblasts. Dentin

matrix protein 1 (DMP1) is a dentin matrix protein that increases predentin width [37]. Dentin sialophosphoprotein (DSPP) is mainly involved in dentin mineralization. DMP1 and DSPP also works reciprocally to ameloblast differentiation [38]. Integrin binding sialoprotein (IBSP), also known as bone sialoprotein (BSP), is important in dentin and cementum mineralization. Collagen type I (encoded by *Col1*) is involved in dentin and dental pulp development in the pre-secretory and secretory stages of odontoblast development [30]. Sonic hedgehog (SHH) is essential in tooth development [28]. The different steps of tooth development result from reciprocality maturation of ectodermal and mesenchymal cells. Malfunction of the corresponding genes affects the differentiation or maturation of these cells. Accordingly, we conducted an exhaustive analysis of gene expression levels in cultured dental bud cells using microarray analysis. The *Alpl* expression decreased the least in *Alpl*$^{-/-}$ mice among subjected genes in our study. In addition, several genes related to tooth development showed significant reduction in *Alpl*$^{-/-}$ mice (Table 1). Our data indicated that lack of *Alpl* gene was associated with reduced expression of all the above-mentioned protein-encoding genes except for *Dmp1*, *Mmp20*, and *Col1*. Hence, *Alpl* deletion results in enamel, dentin, and cementum mineralization abnormalities in *Alpl*$^{-/-}$ mice.

AMELX accounts for ~90% of the enamel protein [18]. During enamel development, AMELX is considered to secure or “hold” space for enamel formation and provide space for hydroxyapatite crystal growth [39]. It is believed that AMELX is an important molecule in the growth and expansion of the enamel layer. *Amelx*$^{-/-}$ mice are characterized by disordered direction of crystals in the enamel rods and enamel dysplasia, i.e., chalky or resembling frosted glass [40]. The enamel thickness of *Amelx*$^{-/-}$ mice was thinner than in wild type. Abnormality of the form and differentiation of ameloblasts in *Amelx*$^{-/-}$ mice is observed [41]. Enamel in *Amelx*$^{-/-}$ mice have more severe abnormality, such as thin enamel and abnormal ameloblasts [40, 41], than those in *Alpl*$^{-/-}$ mice we used. On the other hand, AMBN and ENAM play a role in ameloblast formation so that *Ambn* or *Enam* knockout mice showed irregulatry of the formation or detachment of ameloblast [42-45]. AMELX, AMBN, and ENAM are known to be associated with the pre-secretory or early secretory stage of amelogenesis [18]. AMBN has been identified as an essential molecule for enamel formation,

directly involved in ameloblast differentiation and adhering to matrix protein secreted by ameloblasts [46]. AMBN is found mostly in newly formed enamel at secretory stage and more so at the outer surface than in deeper areas closest to dentinoenamel junction [18]. In our IHC, AMBN was detected at corresponding enamel areas to the same extent in both *Alpl*$^{+/+}$ and *Alpl*$^{-/-}$ mice. *Ambn*$^{-/-}$ mice have enamel hypoplasia that is more severe than in *Amelx*$^{-/-}$ mice, with a complete loss of enamel structure [42, 47]. It had been shown that *Amelx* expression was significantly decreased in *Ambn*$^{-/-}$ mice, whereas *Ambn* expression was largely unaffected in these mice. Based on the above, it is also believed that AMBN plays a central role in the secretion of several EMPs by ameloblasts. Despite expression of *Ambn* was low in *Alpl*$^{-/-}$ mice, there was no significant difference in that of *Amelx* between *Alpl*$^{+/+}$ and *Alpl*$^{-/-}$ mice in our result. In *Alpl*$^{-/-}$ mice on day 5, the expression of *Ambn* may be enough to induce normal expression of *Amelx*.The function of ENAM in enamel mineralization has not yet been established. Multi-layered ameloblasts and disturbance of enamel organ structure in the early stages of teeth development, with uninitiated enamel formation have been reported in *Enam*-mutant mice [48]. Therefore, ENAM is considered an important molecule for ameloblast stability and the initiation of enamel formation [49, 50].

Ambn and *Enam* mRNA expressions were significantly lower in *Alpl*$^{-/-}$ mice than those of *Alpl*$^{+/+}$ mice using qPCR. However, despite the significant difference in microarray analysis, the *Amelx* expression was not altered in qPCR analysis. This may have caused by the differences of their expression profilings between mRNA and protein, and by the developmental stage of their used samples. Histologically, the *Alpl*$^{-/-}$ mice showed presence of a thin, rough, and partly reduced enamel layer compared with *Alpl*$^{+/+}$ mice. The ameloblasts arranged irregularly in alignment and showed aberrant nuclear transition along the enamel layer. Immunohistochemical analysis revealed that *Alpl*$^{-/-}$ mice had the lopsided distribution of Amelx, Ambn, and Enam compared with *Alpl*$^{+/+}$ mice. The enamel organ at bell stage showed the final shape of crown, and the ameloblasts to form enamel [18]. Therefore, we considered that the enamel defects of *Alpl*$^{-/-}$ mice may be caused by the disturbance of ameloblast function with the aberrant expression and distribution of Amelx, Ambn, and Enam proteins. Hence, these EMPs are likely linked with the enamel defect observed in *Alpl*$^{-/-}$ mice.

In summary, ALP activity defectives were shown in stratum intermedium, stellate reticulum, odontoblast and dental pulp in *Alpl*$^{-/-}$ mice in day 5. The stratum intermedium and odontoblast are associated with ameloblast in early amelogenesis stage by epithelial-mesenchymal cells of sequential and reciprocal tooth development. In biological and histological analysis of day 5 *Alpl*$^{-/-}$ mice, EMPs expression levels decreased in tooth germs and the H&E staining showed the aberrance of ameloblasts. These results provided evidence that *Alpl* may involve amelogenesis, such as ameloblast differentiation and EMPs expression.

Based on the previous studies and the current study of *Alpl*$^{-/-}$ mice, we suggest that the loss of TNSALP leads to enamel defects as a result of aberrant ameloblast formation and reduced expression of EMP-encoding genes. Our study advances elucidation of the mechanisms that underlie enamel development, and will help establish the causes of enamel defects of HPP patients.

Disclosures

Both authors declare that no conflict of interest exists.

Acknowledgments

We thank Prof. Takehiko Shimizu for technical support and for assistance in preparation of this manuscript and Dr. Takashi Uchida (Hiroshima University) for providing the Enam rabbit antiserum. This research was supported by JSPS KAKENHI Grant Number JP25862035 and JP16K20658 and a grant from the Research Institute of Oral Science, Nihon University School of Dentistry at Matsudo.

References

1. Linglart A, Biosse-Duplan M: Hypophosphatasia. Curr Osteoporos Rep, 14: 95-105, 2016.

2. Mornet E: Hypophosphatasia. Orphanet J Rare Dis, 2: 40, 2007.

3. Wei KW, Xuan K, Liu YL, Fang J, Ji K, Wang X, Jin Y, Watanabe S, Watanabe K, Ojihara T: Clinical, pathological and genetic evaluations of Chinese patients with autosomal-dominant hypophosphatasia. Arch Oral Biol, 55: 1017-1023, 2010.

4. McKee MD, Hoac B, Addison WN, Barros NM, Millán JL, Chaussain C: Extracellular matrix mineralization in periodontal tissues: Noncollagenous matrix proteins, enzymes, and relationship to hypophosphatasia and X-linked hypophosphatemia. Periodontol 2000, 63: 102-122, 2013.

5. Bloch-Zupan A: Hypophosphatasia: diagnosis and clinical signs - a dental surgeon perspective. Int J Paediatr Dent, 26:426-438, 2016.

6. Millán JL, Narisawa S, Lemire I, Loisel TP, Boileau G, Leonard P, Gramatikova S, Terkeltaub R, Camacho NP, McKee MD, Crine P, Whyte MP: Enzyme replacement therapy for murine hypophosphatasia. J Bone Miner Res, 23: 777-787, 2008.

7. Yamamoto S, Orimo H, Matsumoto T, Iijima O, Narisawa S, Maeda T, Millán JL, Shimada T: Prolonged survival and phenotypic correction of *Akp2*$^{-/-}$ hypophosphatasia mice by lentiviral gene therapy. J Bone Miner Res, 26: 135-142, 2011.

8. Foster BL, Nagatomo KJ, Nociti FH Jr, Fong H, Dunn D, Tran AB, Wang W, Narisawa S, Millán JL, Somerman MJ: Central role of pyrophosphate in acellular cementum formation. PLoS One, 7: e38393, 2012.

9. Zweifler LE, Patel MK, Nociti FH Jr, Wimer HF, Millán JL, Somerman MJ, Foster BL: Counter-regulatory phosphatases TNAP and NPP1 temporally regulate tooth root cementogenesis. Int J Oral Sci, 7: 27-41, 2015.

10. Foster BL, Nagatomo KJ, Tso HW, Tran AB, Nociti FH Jr, Narisawa S, Yadav MC, McKee MD, Millán JI, Somerman MJ: Tooth root dentin mineralization defects in a mouse model of hypophosphatasia. J Bone Miner Res, 28: 271-282, 2013.

11. Yadav MC, de Oliveira RC, Foster BL, Fong H, Cory E, Narisawa S, Sah RL, Somerman

M, Whyte MP, Millán JL: Enzyme replacement prevents enamel defects in hypophosphatasia mice. J Bone Miner Res, 27: 1722-1734, 2012.

12. Narisawa S, Fröhlander N, Millán JL: Inactivation of two mouse alkaline phosphatase genes and establishment of a model of infantile hypophosphatasia. Dev. Dyn, 208: 432-446, 1997.

13. Matsumoto T, Miyake K, Yamamoto S, Orimo H, Miyake N, Odagaki Y, Adachi K, Iijima O, Narisawa S, Millán JL, Fukunaga Y, Shimada T: Rescue of severe infantile hypophosphatasia mice by AAV-mediated sustained expression of soluble alkaline phosphatase. Hum Gene Ther, 22: 1355-1364, 2011.

14. Ogawa N, Shimizu K: *Fgf20* and *Fgf4* may contribute to tooth agenesis in epilepsy-like disorder mice. Ped Den J, 26: 21-27, 2016.

15. Uchida T, Tanabe T, Fukae M, Shimizu M, Yamada M, Miake K, Kobayashi S: Immunochemical and immunohistochemical studies, using antisera against porcine 25 kDa amelogenin, 89 kDa enamelin and the 13-17 kDa nonamelogenins, on immature enamel of the pig and rat. Histochemistry, 96: 129-138, 1991.

16. Osmundsen H, Landin MA, From SH, Kolltveit KM, Risnes S: Changes in gene-expression during development of the murine molar tooth germ. Arch Oral Biol, 52:803-813, 2007.

17. Landin MA, Shabestari M, Babaie E, Reseland JE, Osmundsen H: Gene expression profiling during murine tooth development. Front Genet, 3: 139, 2012.

18. Nanci A: Ten Cate's Oral Histology Development, Structure, and Function, 8th ed, 2013, Elsevier Mosby, St. Louis, MO.

19. Hu JC, Simmer JP: Developmental biology and genetics of dental malformations. Orthod Craniofac Res, 10: 45-52, 2007.

20. Rauth RJ, Potter KS, Ngan AY, Saad DM, Mehr R, Luong VQ, Schuetter VL, Miklus VG, Chang P, Paine ML, Lacruz RS, Snead ML, White SN: Dental enamel: genes define biomechanics. J Calif Dent Assoc, 37: 863-868, 2009.

21. Hu JC, Chun YH, Al Hazzazzi T, Simmer JP: Enamel formation and amelogenesis imperfecta. Cells Tissues Organs, 186:78-85, 2007.

22. Lacruz RS, Nakayama Y, Holcroft J, Nguyen V, Somogyi-Ganss E, Snead ML, White SN, Paine ML, Ganss B: Targeted overexpression of amelotin disrupts the microstructure of dental enamel. PLoS One, 7: e35200, 2012.

23. Nakayama Y, Holcroft J, Ganss B: Enamel hypomineralization and structural defects in amelotin-deficient mice. J Dent Res, 94: 697-705, 2015.

24. Wazen RM, Moffatt P, Ponce KJ, Kuroda S, Nishio C, Nanci A: Inactivation of the Odontogenic ameloblast-associated gene affects the integrity of the junctional epithelium and gingival healing. Eur Cell Mater, 30: 187-199, 2015.

25. Hu Y, Hu JC, Smith CE, Bartlett JD, Simmer JP: Kallikrein-related peptidase 4, matrix metalloproteinase 20, and the maturation of murine and porcine enamel. Eur J Oral Sci, 119: 217-225, 2011.

26. Sreenath T, Thyagarajan T, Hall B, Longenecker G, D'Souza R, Hong S, Wright JT, MacDougall M, Sauk J, Kulkarni AB: Dentin sialophosphoprotein knockout mouse teeth display widened predentin zone and develop defective dentin mineralization similar to human dentinogenesis imperfecta type III. J Biol Chem, 278: 24874-24880, 2003.

27. Foster BL, Soenjaya Y, Nociti FH Jr, Holm E, Zerfas PM, Wimer HF, Holdsworth DW, Aubin JE, Hunter GK, Goldberg HA, Somerman MJ: Deficiency in acellular cementum and periodontal attachment in *Bsp* null mice. J Dent Res, 92: 166-172, 2013.

28. Balic A, Thesleff I: Tissue interactions regulating tooth development and renewal. Curr Top Dev Biol, 115: 157-186, 2015.

29. Rangiani A, Cao ZG, Liu Y, Voisey Rodgers A, Jiang Y, Qin CL, Feng JQ: Dentin matrix protein 1 and phosphate homeostasis are critical for postnatal pulp, dentin and enamel formation. Int J Oral Sci, 4: 189-195, 2012.

30. He P, Zhang Y, Kim SO, Radlanski RJ, Butcher K, Schneider RA, DenBesten PK: Ameloblast differentiation in the human developing tooth: effects of extracellular matrices. Matrix Biol, 29: 411-419, 2010.

31. Zhang Z, Tian H, Lv P, Wang W, Jia Z, Wang S, Zhou C, Gao X: Transcriptional factor DLX3 promotes the gene expression of enamel matrix proteins during amelogenesis. PLoS One, 10: e0121288, 2015.

32. Liu J, Nam HK, Campbell C, Gasque KC, Millán JL, Hatch NE: Tissue-nonspecific alkaline phosphatase deficiency causes abnormal craniofacial bone development in the *Alpl*$^{-/-}$ mouse model of infantile hypophosphatasia. Bone, 67: 81-94, 2014.

33. Wise GE, Fan W: Changes in the tartrate-resistant acid phosphatase cell population in dental follicles and bony crypts of rat molars during tooth eruption. J Dent Res, 68:150-156, 1989.

34. Koyama E, Wu C, Shimo T, Iwamoto M, Ohmori T, Kurisu K, Ookura T, Bashir MM, Abrams WR, Tucker T, Pacifici M: Development of stratum intermedium and its role as a *Sonic hedgehog*-signaling structure during odontogenesis. Dev Dyn, 222: 178-191, 2001.

35. Gritli-Linde A, Bei M, Maas R, Zhang XM, Linde A, McMahon AP: Shh signaling within the dental epithelium is necessary for cell proliferation, growth and polarization. Development, 129:5323-5337, 2002.

36. Gritli-Linde A, Lewis P, McMahon AP, Linde A: The whereabouts of a morphogen: direct evidence for short- and graded long-range activity of hedgehog signaling peptides. Dev Biol, 236: 364-386, 2001.

37. Lu Y, Ye L, Yu S, Zhang S, Xie Y, McKee MD, Li YC, Kong J, Eick JD, Dallas SL, Feng JQ: Rescue of odontogenesis in *Dmp1*-deficient mice by targeted re-expression of DMP1 reveals roles for DMP1 in early odontogenesis and dentin apposition *in vivo*. Dev Biol, 303:191-201, 2007.

38. Ye L, MacDougall M, Zhang S, Xie Y, Zhang J, Li Z, Lu Y, Mishina Y, Feng JQ: Deletion of dentin matrix protein-1 leads to a partial failure of maturation of predentin into dentin, hypomineralization, and expanded cavities of pulp and root canal during postnatal tooth development. J Biol Chem, 279:19141-19148, 2004.

39. Diekwisch T, David S, Bringas P Jr, Santos V, Slavkin HC: Antisense inhibition of AMEL translation demonstrates supramolecular controls for enamel HAP crystal growth during embryonic mouse molar development. Development , 117: 471-482, 1993.

40. Gibson CW, Yuan ZA, Hall B, Longenecker G, Chen E, Thyagarajan T, Sreenath T, Wright JT, Decker S, Piddington R, Harrison G, Kulkarni AB: Amelogenin-deficient mice display an amelogenesis imperfecta phenotype. J Biol Chem, 276: 31871-31875, 2001.

41. Cho ES, Kim KJ, Lee KE, Lee EJ, Yun CY, Lee MJ, Shin TJ, Hyun HK, Kim YJ, Lee SH, Jung HS, Lee ZH, Kim JW.: Alteration of conserved alternative splicing in AMELX causes enamel defects. J Dent Res, 93: 980-987, 2014.

42. Hatakeyama J, Fukumoto S, Nakamura T, Haruyama N, Suzuki S, Hatakeyama Y, Shum L, Gibson CW, Yamada Y, Kulkarni AB: Synergistic roles of amelogenin and ameloblastin. J Dent Res, 88: 318-322, 2009.

43. Jacques J, Hotton D, De la Dure-Molla M, Petit S, Asselin A, Kulkarni AB, Gibson CW, Brookes SJ, Berdal A, Isaac J: Tracking endogenous amelogenin and ameloblastin *in vivo*. PLoS One, 9:e99626, 2014.

44. Sawada T, Sekiguchi H, Uchida T, Yamashita H, Shintani S, Yanagisawa T.:Histological and immunohistochemical analyses of molar tooth germ in enamelin-deficient mouse. Acta Histochem, 113: 542-546, 2011.

45. Smith CE, Wazen R, Hu Y, Zalzal SF, Nanci A, Simmer JP, Hu JC: Consequences for enamel development and mineralization resulting from loss of function of ameloblastin or enamelin. Eur J Oral Sci, 117: 485-497, 2009.

46. Fukumoto S, Kiba T, Hall B, Iehara N, Nakamura T, Longenecker G, Krebsbach PH, Nanci A, Kulkarni AB, Yamada Y: Ameloblastin is a cell adhesion molecule required for maintaining the differentiation state of ameloblasts. J Cell Biol, 167:973-983, 2004.

47. Chun YH, Lu Y, Hu Y, Krebsbach PH, Yamada Y, Hu JC, Simmer JP: Transgenic rescue of enamel phenotype in Ambn null mice. J Dent Res, 89: 1414-1420, 2010.

48. Hu JC, Hu Y, Lu Y, Smith CE, Lertlam R, Wright JT, Suggs C, McKee MD, Beniash E, Kabir ME, Simmer JP: Enamelin is critical for ameloblast integrity and enamel ultrastructure formation. PLoS One, 9: e89303, 2014.

49. Masuya H, Shimizu K, Sezutsu H, Sakuraba Y, Nagano J, Shimizu A, Fujimoto N, Kawai A, Miura I, Kaneda H, Kobayashi K, Ishijima J, Maeda T, Gondo Y, Noda T, Wakana S, Shiroishi T: Enamelin (Enam) is essential for amelogenesis: ENU-induced mouse mutants as models for different clinical subtypes of human amelogenesis imperfecta (AI). Hum Mol Genet , 14: 575-583, 2005.

50. Hu JC, Hu Y, Smith CE, McKee MD, Wright JT, Yamakoshi Y, Papagerakis P, Hunter GK,

Feng JQ, Yamakoshi F, Simmer JP: Enamel defects and ameloblast-specific expression in *Enam* knock-out/*lacz* knock-in mice. J Biol Chem, 283: 10858-10871, 2008.

Captions

Fig. 1. H&E staining of M1s germs of *Alpl*$^{+/+}$ and *Alpl*$^{-/-}$ mice on postnatal day 5. A. Lower magnification of M1, *Alpl*$^{+/+}$ mouse. B, C. Higher magnification of areas marked in A (crown). D. Low magnification of M1, *Alpl*$^{-/-}$ mouse. E, F. Higher magnification of areas marked in D (crown). Irregular ameloblasts (asterisk), partial lack of enamel, uneven form, and rippling layers (arrow heads) are apparent. The images are representative of 5 samples from each group animals. eo; enamel organ, sr; stellate reticulum, si; stratum intermedium, a; ameloblasts, e; enamel, d; dentin, pd; predentin, o; odontoblasts, dp; dental pulp, scale bars = 100 μm (A, D) and 50 μm (B, C, E, F).

Fig. 2. ALP activity of the craniofacial regions of *Alpl*$^{+/+}$ and *Alpl*$^{-/-}$ mice on postnatal day 5. A. Lower magnification of the M1 area in *Alpl*$^{+/+}$ mice. B. Higher magnification micrographs of areas marked in A. C. Lower magnification of the M1 area in *Alpl*$^{-/-}$ mice. D. Higher magnification micrographs of areas marked in C. The images are representative of 5 samples from each group animals. sr; stellate reticulum, si; stratum intermedium, a; ameloblasts, e; enamel, d; dentin, pd; predentin, o; odontoblasts, scale bars = 100 μm.

Fig. 3. IHC staining of AMELX of M1s germs of *Alpl*$^{+/+}$ and *Alpl*$^{-/-}$ mice on postnatal day 5. A. Lower magnification of M1 in *Alpl*$^{+/+}$ mice. B, C. Higher magnification of areas marked in A (crown). D–F. Negative control (rabbit IgG) for *Alpl*$^{+/+}$ mouse tissue staining. G. Low magnification of M1 in *Alpl*$^{-/-}$ mice. H, I. Higher magnification of areas marked in G (crown). J–L. Negative control (rabbit IgG) for *Alpl*$^{-/-}$ mouse tissue staining. The images are representative of 1 sample from each group animals. eo; enamel organ, sr; stellate reticulum, si; stratum intermedium, a; ameloblasts, e; enamel, d; dentin, pd; predentin, o; odontoblasts,

dp; dental pulp, scale bars = 100 μm (A, D, G, J) and 50 μm (B, C, E, F, H, I, K, L).

Fig. 4. IHC staining of AMBN of M1s germs in *Alpl*$^{+/+}$ and *Alpl*$^{-/-}$ mice on postnatal day 5. A. Lower magnification of M1 in *Alpl*$^{+/+}$ mice. B, C. Higher magnification of areas marked in A (crown). D–F. Negative control (rabbit IgG) for *Alpl*$^{+/+}$ mouse tissue staining. G. Low magnification of M1 in *Alpl*$^{-/-}$ mice. H, I. Higher magnification of areas marked in G (crown). J–L. Negative control (rabbit IgG) for *Alpl*$^{-/-}$ mouse tissue staining. The images are representative of 1sample from each group animals. eo; enamel organ, sr; stellate reticulum, si; stratum intermedium, a; ameloblasts, e; enamel, d; dentin, pd; predentin, o; odontoblasts, dp; dental pulp, scale bars = 100 μm (A, D, G, J) and 50 μm (B, C, E, F, H, I, K, L).

Fig. 5. IHC staining of ENAM of M1s germs in *Alpl*$^{+/+}$ and *Alpl*$^{-/-}$ mice on postnatal day 5. A. Lower magnification of M1 in *Alpl*$^{+/+}$ mice. B, C. Higher magnification of areas marked in A (crown). D–F. Negative control (normal rabbit serum) for *Alpl*$^{+/+}$ mouse tissue staining. G. Low magnification of M1 in *Alpl*$^{-/-}$ mice. H, I. Higher magnification of areas marked in G (crown). J–L. Negative control (rabbit IgG) for *Alpl*$^{-/-}$ mouse tissue staining. The images are representative of 1 sample from each group animals. eo; enamel organ, sr; stellate reticulum, si; stratum intermedium, a; ameloblasts, e; enamel, d; dentin, pd; predentin, o; odontoblasts, dp; dental pulp, scale bars = 100 μm (A, D, G, J) and 50 μm (B, C, E, F, H, I, K, L).

Fig. 6. Relative abundances of genes associated with tooth development. The expression of *Amelx* (A), *Ambn* (B), and *Enam* (C) in M1s at late bell stage *Alpl*$^{+/+}$ and *Alpl*$^{-/-}$ mice on postnatal day 5. Gene expression relative to *Gapdh* is presented as the mean ± SD from in triplicate. Mann-Whitney U test was used to determine differences between groups; *$p < 0.05$; **$p < 0.01$ ($n = 5$ for each mouse group).

Table 1. Gene expression ratio in *Alpl*$^{-/-}$ mice compared with that in *Alpl*$^{+/+}$ mice by microarray analysis.

Rank	Log_2 Ratio	Gene Symbol	GenBank® Accession number	Annotations
1	-7.32	***Alpl***	[NM_007431]	alkaline phosphatase, liver/bone/kidney
2	-6.21	***Amelx***	[NM_009666]	amelogenin, X-linked
3	-3.72	***Amtn***	[NM_027793]	amelotin
4	-2.72	***Enam***	[NM_017468]	enamelin
5	-2.11	***Ibsp***	[NM_008318]	integrin binding sialoprotein
6	-1.78	***Odam***	[NM_027128]	odontogenic, ameloblast asssociated
7	-1.75	***Klk4***	[NM_019928]	kallikrein related-peptidase 4
8	-1.34	***Ambn***	[NM_001303431]	ameloblastin
9	-1.06	***Dspp***	[NM_010080]	dentin sialophosphoprotein
10	-1.01	***Shh***	[NM_009170]	sonic hedgehog

Fig. 1.

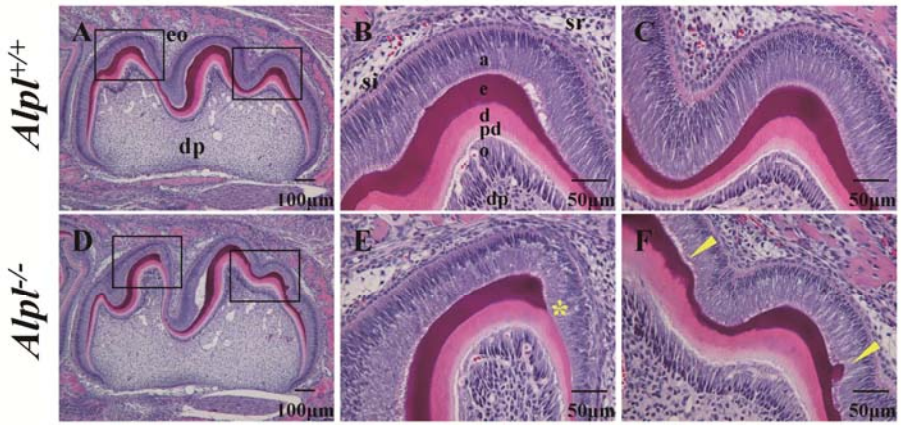
Alpl+/+
Alpl-/-
A
eo
dp
100μm
B
sr
a
si
e
d
pd
o
dp
50μm
C
50μm
D
100μm
E
50μm
F
50μm

Fig. 2.

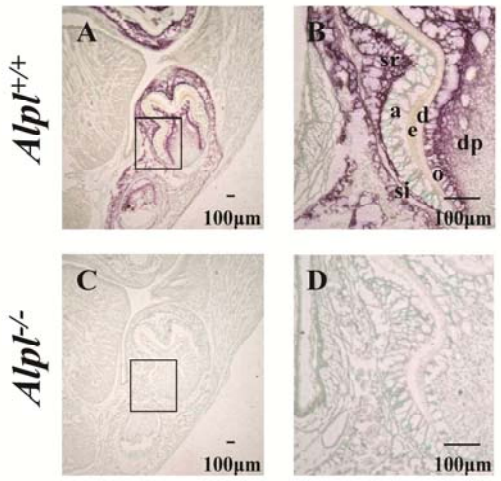
Alpl+/+
Alpl-/-
A
100μm
B
sr
a
d
e
dp
o
si
100μm
C
100μm
D
100μm

Fig. 3.

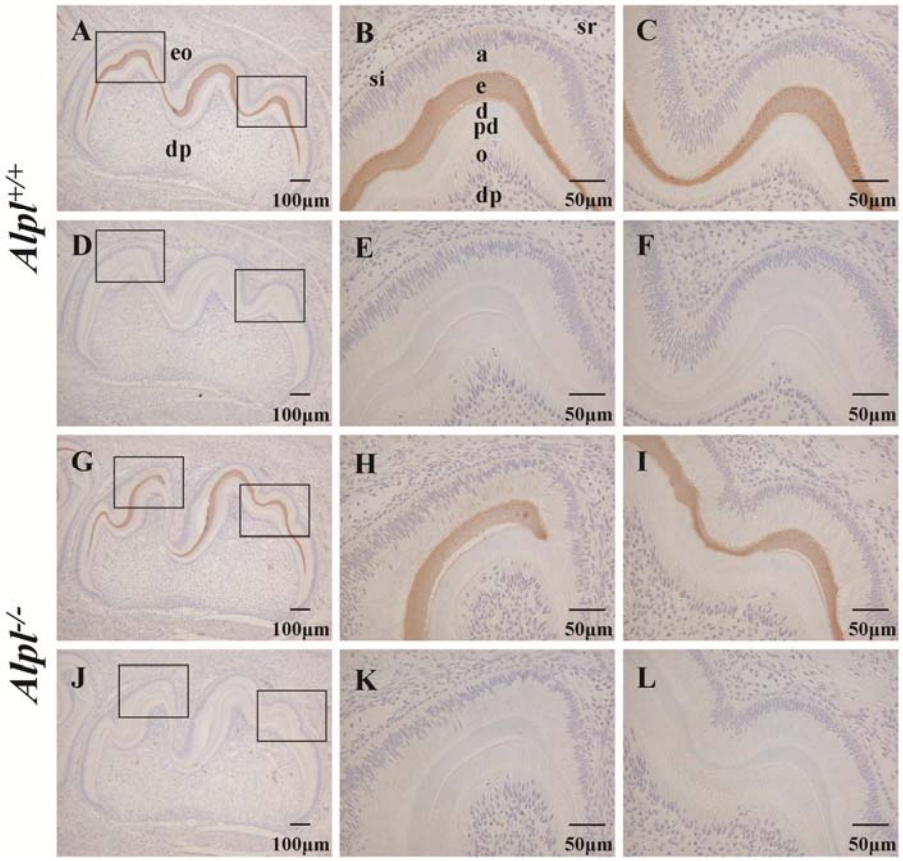
Alpl+/+
Alpl-/-
A
eo
dp
100μm
B
sr
si
a
e
d
pd
o
dp
50μm
C
50μm
D
100μm
E
50μm
F
50μm
G
100μm
H
50μm
I
50μm
J
100μm
K
50μm
L
50μm

Fig. 4.

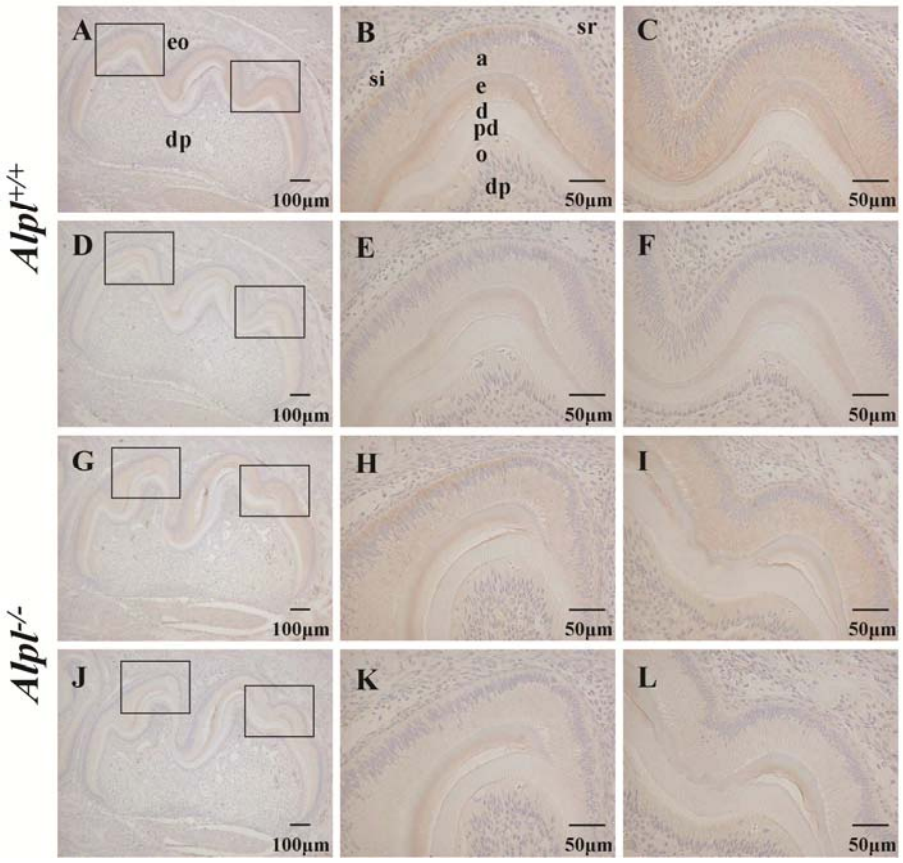
Alpl+/+
Alpl-/-
A
eo
dp
100μm
B
sr
si
a
e
d
pd
o
dp
50μm
C
50μm
D
100μm
E
50μm
F
50μm
G
100μm
H
50μm
I
50μm
J
100μm
K
50μm
L
50μm

Fig. 5.

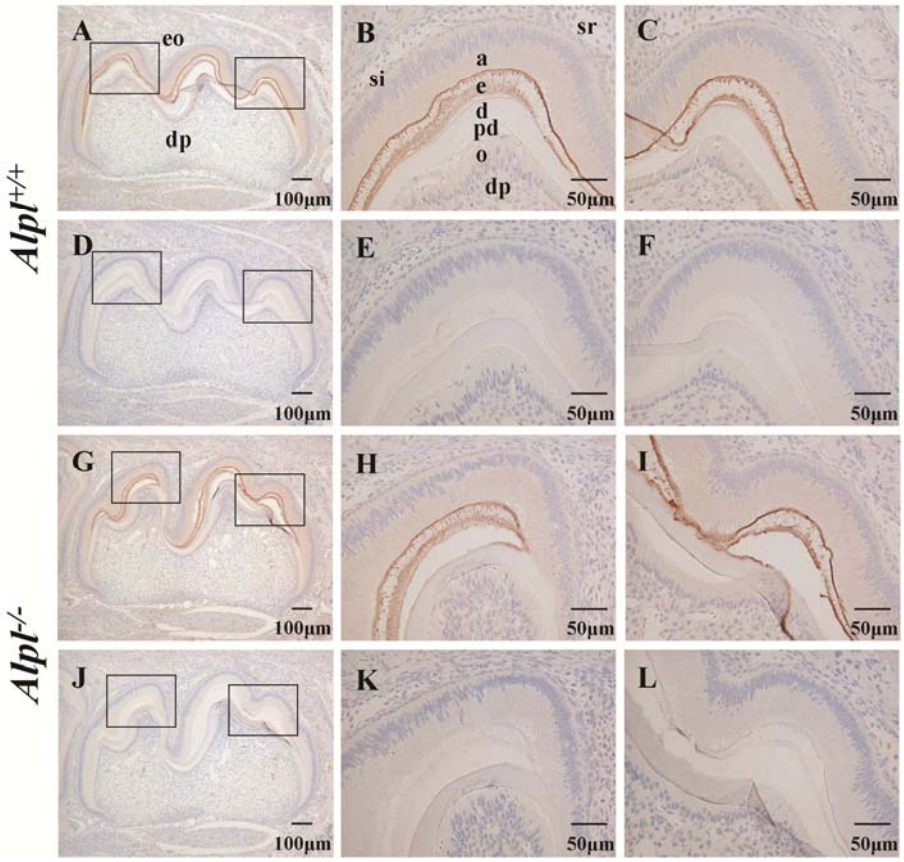
Alpl+/+
Alpl-/-
A
eo
dp
100μm
B
sr
si
a
e
d
pd
o
dp
50μm
C
50μm
D
100μm
E
50μm
F
50μm
G
100μm
H
50μm
I
50μm
J
100μm
K
50μm
L
50μm

Fig. 6.

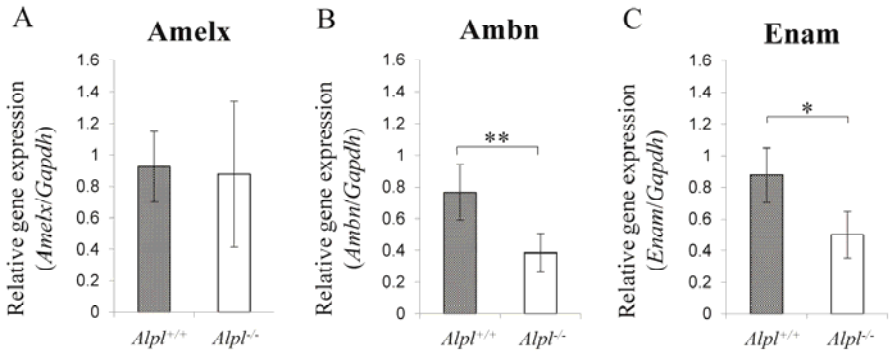
A
Amelx
Relative gene expression (Amelx/Gapdh)
1.6
1.4
1.2
1
0.8
0.6
0.4
0.2
0
Alpl+/+
Alpl-/-
B
Ambn
Relative gene expression (Ambn/Gapdh)
**
C
Enam
Relative gene expression (Enam/Gapdh)
*